

05
Investigation of spectral characteristics of plasma jet during laser ablation of calcium hydroxyapatite

© Yu.D. Dudnik, M.I. Vasilyev, A.A. Safronov, V.N. Shiryayev, O.B. Vasilieva

Institute for Electrophysics and Electric Power of the Russian Academy of Sciences
St. Petersburg, Russia
e-mail: milavas@mail.ru; julia_dudnik-s@mail.ru

Received April 29, 2025

Revised June 19, 2025

Accepted October 24, 2025

The results of a plasma jet analysis are presented during the deposition of calcium hydroxyapatite $\text{Ca}_{10}(\text{PO}_4)_6(\text{OH})_2$ coatings on Ti–6Al–4V substrates via laser ablation of targets with a KrF excimer laser. The deposition was performed under an oxygen pressure of 10^{-4} Torr in a vacuum chamber at room temperature. During the ablation process, emission spectra were recorded using two fast spectrophotometers in the 268–674 nm range. A comparative analysis of the spectroscopic data is performed, and the results of color image processing and the characteristics of the plasma jet propagation during ablation are estimated.

Keywords: pulsed laser deposition, laser ablation, thin films, plasma jet, emission spectra.

DOI: 10.61011/EOS.2025.10.62555.7927-25

Introduction

Calcium hydroxyapatite $\text{Ca}_{10}(\text{PO}_4)_6(\text{OH})_2$ (hereinafter HAP) is the main chemical component of bone tissue (70%) [1] and can be used as a coating for dental and orthopedic metal implants and prostheses. Due to its unique properties, HAP is considered a promising material for developing various types of biomedical structures [1–4]. HAP represents a bioactive substance that promotes optimal interaction between artificial implants and living bone tissue, making it an indispensable component in the production of implantation devices not subject to mechanical loads. Due to its increased brittleness, bulk HAP-based ceramics are unsuitable for manufacturing dental and orthopedic products that experience intense mechanical stress throughout their expected service life [1,2]. These shortcomings can be eliminated by applying thin HAP coatings onto biocompatible high-strength metals or alloys [3]. Over the past decade, various coating deposition methods have been used to obtain HAP coatings with desired characteristics [2–6], with pulsed laser deposition (PLD) proving to be one of the most promising. In 1992, PLD HAP films on Ti–6Al–4V substrates were reported for the first time. Since then, several studies have been conducted in various atmospheres (Ar, O_2 , H_2O and their combinations) to produce ideal implants [6,7]. The PLD method allows good control of crystallinity with various compositions and phases, even with HAP as the sole phase.

In the present work, an analysis of the plasma plume during HAP coating deposition was conducted to produce pure, adherent, and crystalline HAP coatings via post-deposition annealing at 300°C of amorphous HAP obtained by PLD at room temperature. The composition and

propagation of the plasma plume, which forms the HAP coating on the substrate, were evaluated.

The goal of this work is to study emission spectra in comparison with results from processing color images of the plasma cloud to analyze plasma plume motion processes.

Experimental procedure

The schematic of the experimental setup shown in Fig. 1 includes a KrF excimer laser, an ultra-high vacuum deposition chamber equipped with a rotating target and fixed substrate holder, and a pumping system consisting of mechanical and turbomolecular pumps. PLD was performed at ambient temperature in a stainless steel vacuum chamber, initially evacuated to a base pressure of 10^{-5} Torr, then filled with oxygen to a processing pressure of 10^{-4} Torr. Commercially available sintered dense HAP disks with a diameter of 27 mm and thickness of 7 mm were used as target materials. Rolled sheets of Ti–6Al–4V ($20 \times 20 \times 0.5$ mm) were used as substrates. Ablation was carried out using a pulsed KrF excimer laser (Lambda Physik EMG 201 MSC) with a wavelength of 248 nm, pulse duration of 20 ns, and repetition rate of 10 Hz. The laser beam was directed onto the HAP target at an incidence angle of 45° with a spot size of 3×1 mm. The laser pulse energy was determined using a pyroelectric detector from the Canadian company Gentec, with an energy density of 3 J/cm^2 .

The ablated material deposits onto the substrate located at a distance of 4–5 cm in front of the laser spot on the target. The average ablation rate [mg/pulse] was measured using high-precision balances (AD-6, Perkin Elmer). The number of laser pulses determined the desired film thickness of

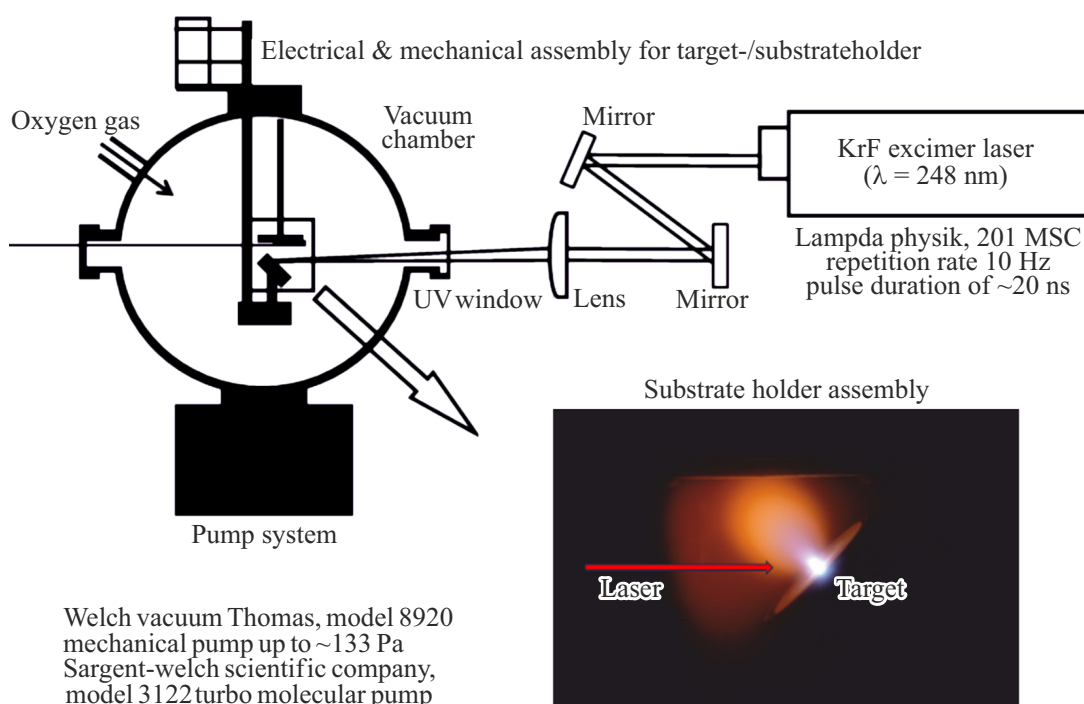


Figure 1. Diagram of the experimental set-up.

approximately $2.5 \mu\text{m}$ corresponding to 25 000 laser pulses, with a deposition rate of about 0.1 nm per pulse. To restore the original crystalline structure, amorphous films obtained by PLD were annealed for 4 h at the following temperatures: 290, 300 and 310°C . Thermal treatment was conducted in air using a horizontal cylindrical furnace. The heating and cooling rates were 5°C min^{-1} .

Results and Discussion

During ablation, emission spectra of the plasma plume were recorded using two fast high-resolution spectrometers (HR 2000+, Ocean Optics Inc.) in the ranges 268–486 and 472–674 nm with a spectral resolution of 0.11 nm and different integration times. The emission spectra obtained with the first spectrometer are shown in Fig. 2, a; the visible region spectrum obtained with the second spectrometer is shown in Fig. 2, b.

The spectrum primarily shows calcium lines Ca I and Ca II. Three lines at wavelengths 315.887, 317.933, and 318.128 nm can be noted, belonging to transitions of the calcium ion Ca II $3p^64p-3p^64d$. Pairs of Ca II lines at 370.603 and 373.690 nm are also observed, belonging to transitions $3p^64p-3p^65s$. Two strong Ca II emission lines at 393.366 and 396.847 nm belong to the transition $3p^64s-3p^64p$ from E_i-E_k $0.00-25414.40 \text{ cm}^{-1}$. In the blue region of the spectrum, a strong Ca I line at 422.673 nm is observed, corresponding to the transition $3p^64s^2-3p^64s4p$ from the zero energy state E_i 0.00 cm^{-1} to E_k $23652.304 \text{ cm}^{-1}$. Energy level schemes for calcium

groups of lines in the visible spectrum region, corresponding to various transitions, are presented in the table.

Color images of KrF excimer laser ablation of HAP targets were recorded using a Nikon D80 digital camera. In the digital camera used, the light flux passes through a Bayer filter — a two-dimensional array of three spatially separated color filters covering the matrix photoreceptor elements. The color image is formed as a result of applying the Bayer filter, consisting of 25% red, 25% blue, and 50% green light filters with corresponding spectral transmission bands.

Image processing of the plasma plume was performed, separately considering the two-dimensional matrices of blue B, green G, and red R colors. A characteristic color image of the plasma plume is shown in Fig. 3, a. As can be seen from Fig. 2, b, in the red part of the spectrum starting from 580 nm, strong emission lines are present, responsible for coloring the plasma plume with the dominant red color. The image was taken through a colorless window in the vacuum chamber and shows the action of a single 248 nm laser pulse with photon energy of 4.999 eV and energy density of 3 J/cm^2 , the exposure corresponded to 10 ms, i.e., one laser operating cycle.

The image recorded by the digital camera in JPG format (truecolor) shown in Fig. 3, a represents an array of three matrices 525–700 that define the red, green, and blue color components for each individual pixel. In Fig. 3, a, 4 lines (profiles) parallel to the target plane are drawn. The lines reflect the brightness state of the plasma plume emission with a step of 7.5 mm from the target. For each line

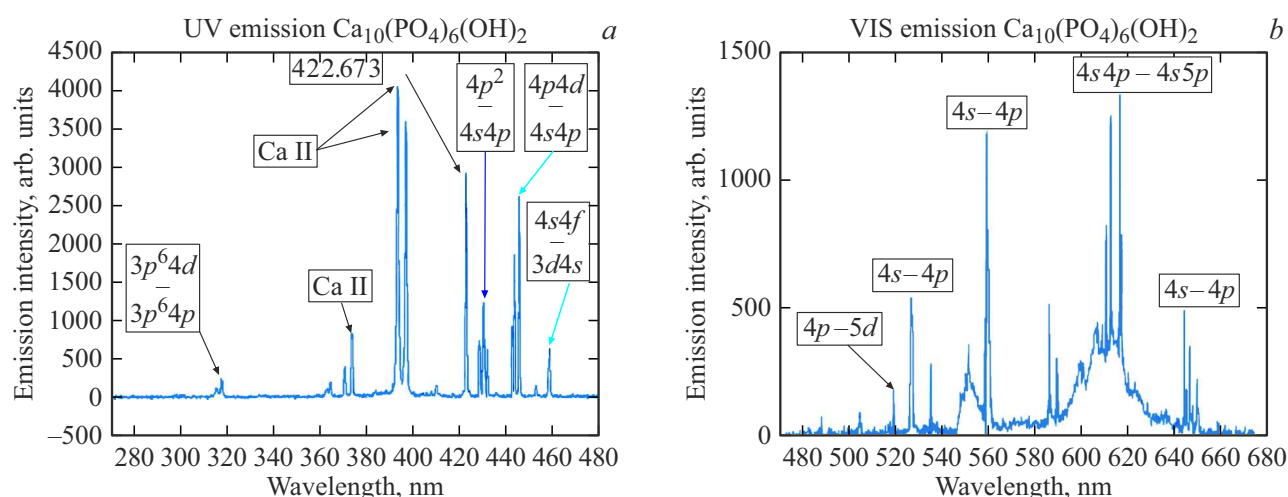


Figure 2. Emission spectrum of the plasma plume during ablation of $\text{Ca}_{10}(\text{PO}_4)_6(\text{OH})_2$: (a) in ultraviolet and blue-green regions, (b) in the visible region.

Table.

Ion	Wavelength, nm	Low – High level
Ca I	526.039	$3p^6 3d4s - 3p^6 3d4p$
Ca I	526.171	$3p^6 3d4s - 3p^6 3d4p$
Ca I	526.224	$3p^6 3d4s - 3p^6 3d4p$
Ca I	526.424	$3p^6 3d4s - 3p^6 3d4p$
Ca I	526.556	$3p^6 3d4s - 3p^6 3d4p$
Ca I	527.027	$3p^6 3d4s - 3p^6 3d4p$
Ca I	558.197	$3p^6 3d4s - 3p^6 3d4p$
Ca I	558.876	$3p^6 3d4s - 3p^6 3d4p$
Ca I	559.012	$3p^6 3d4s - 3p^6 3d4p$
Ca I	559.447	$3p^6 3d4s - 3p^6 3d4p$
Ca I	559.849	$3p^6 3d4s - 3p^6 3d4p$
Ca I	560.129	$3p^6 3d4s - 3p^6 3d4p$
Ca I	560.285	$3p^6 3d4s - 3p^6 3d4p$
Ca I	643.907	$3p^6 3d4s - 3p^6 3d4p$
Ca I	644.981	$3p^6 3d4s - 3p^6 3d4p$
Ca I	645.560	$3p^6 3d4s - 3p^6 3d4p$
Ca I	646.257	$3p^6 3d4s - 3p^6 3d4p$
Ca I	647.166	$3p^6 3d4s - 3p^6 3d4p$
Ca I	649.378	$3p^6 3d4s - 3p^6 3d4p$
Ca I	649.965	$3p^6 3d4s - 3p^6 3d4p$

(profile), the pixel intensity magnitudes in red, green, and blue colors can be obtained, as shown in Fig. 3, b. As

can be seen, the blue color profile decreases in magnitude and broadens in FWHM (full width at half maximum) with distance from the target (1 line to 4 line). This indicates the expansion of the ablated HAP target products. The expansion angle can be calculated in first approximation from the FWHM magnitude for all lines: 1 line–4 line (for 1 line, extrapolating the upper part of the profile using a spline function). The estimate shows that the angle is $\sim 18\text{--}20^\circ$. A more complex pattern is observed for the green and red profiles. Thus, it can be assumed that Ca II ions relax from the excited to the ground state with emission in the red and green spectral regions. Analysis of the plasma plume image processing results in Fig. 4 confirms the complex spatial character of HAP ablation product propagation.

Conclusion

Emission spectra of the plasma plume formed during laser ablation of calcium hydroxyapatite $\text{Ca}_{10}(\text{PO}_4)_6(\text{OH})_2$ in the range 268–674 nm and color images of the plasma presented as three matrices $m \times n$ (525×700) defining red, green, and blue images were obtained. Asymmetric mushroom-shaped spatial regions with enhanced emission in the red spectral region are observed, while no such regions appear in the blue images, with an expansion angle of the evaporation products of $\sim 18^\circ$. A possible explanation for the asymmetric pattern in the R (red) and G (green) color images consists in the relaxation of Ca II ions from the excited to the ground state, which increases the number of radiative transitions in the red and green regions. The use of multispectral images opens new prospects for in-depth analysis of the spectral properties of the plasma plume.

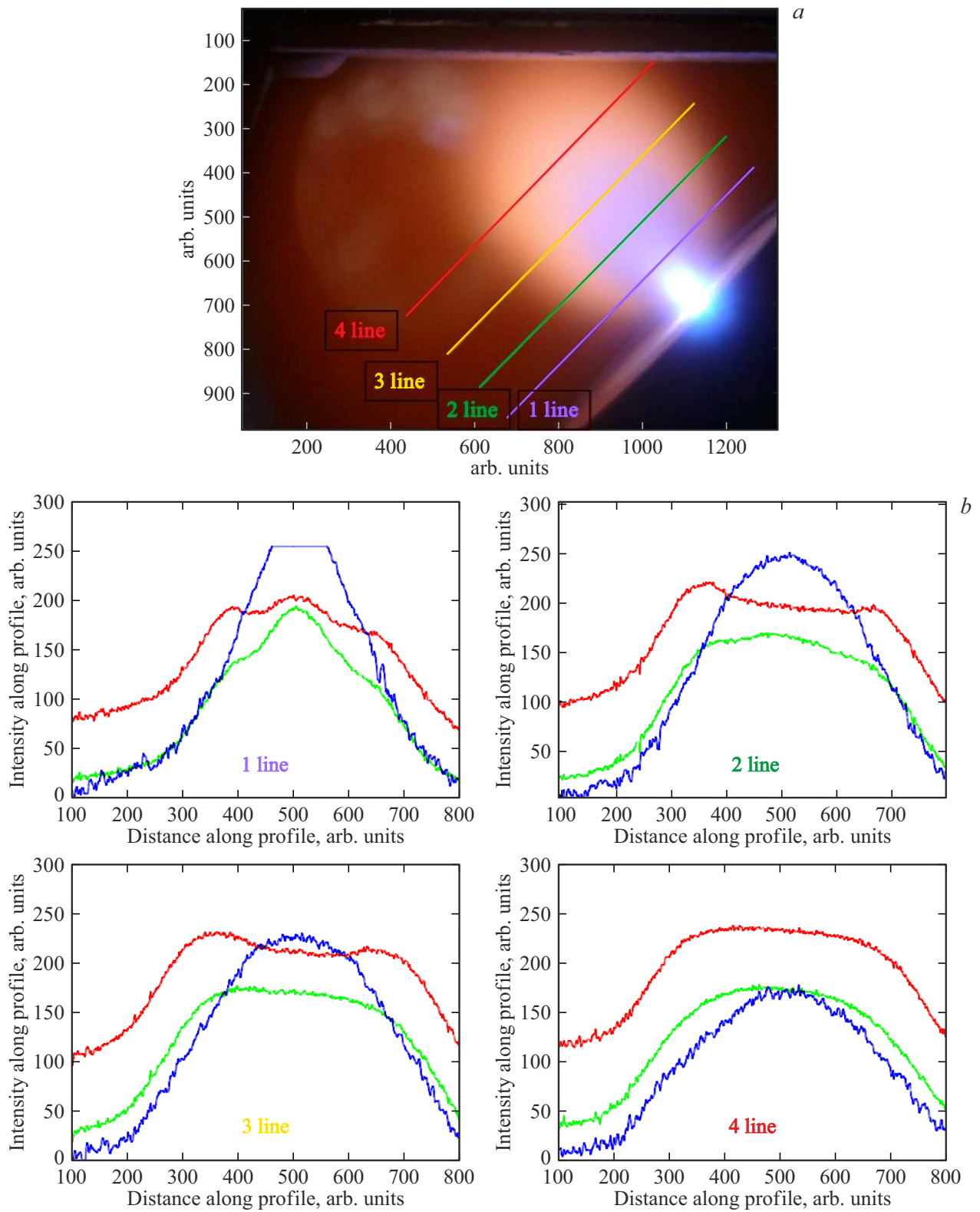


Figure 3. (a) RGB (truecolor) image of a single plasma plume, (b), pixel intensities in red, green, and blue colors along 1, 2, 3, and 4 lines.

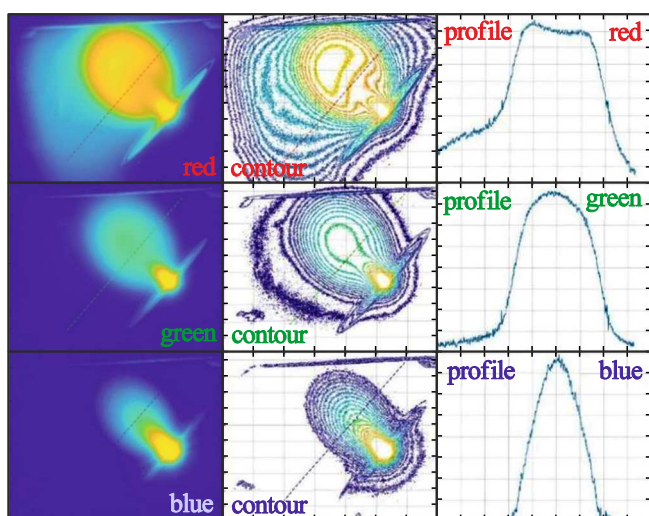


Figure 4. Images from top to bottom R, G, B of a single plasma plume: left column — images in artificial palette, middle column — contours of R, G, B images, right — pixel intensities along the indicated line in R, G, and B colors.

Conflict of interest

The authors declare that they have no conflict of interest.

References

- [1] S. Kylychbekov, Y. Allamyradov, Z. Khuzhakulov, I. Majidov, S. Banga, J. Yosef, L. Duta, A.Er. *Coatings*, **13** (10), 1681 (2023). DOI: 10.3390/coatings13101681
- [2] N.A. Zakharov, E.M. Koval', A.D. Aliev, E.V. Shelekhov, M.R. Kiselyov, V.V. Matveev, M.A. Orlov, L.I. Dyomina, T.V. Zakharova, N.T. Kuznetsov. *Zhurn. neorgan. khimii*, **66** (3), 317 (2021). (in Russian). DOI: 10.31857/S0044457X21030211
- [3] T.R. Chueva, N.V. Gamurar, V.I. Kalita, D.I. Komlev, A.A. Radyuk, V.S. Komlev, A.Yu. Teterina, V.F. Shamraj, A.B. Mikhajlova. *Perspektivnye materialy*, **8**, 33 (2021). (in Russian). DOI: 10.30791/1028-978X-2021-8-33-43
- [4] A.S. Chekueva, Ch.B. Daulbaev, F.R. Sultanov, B. Bakbolat, R.I. Gadylyshina. *Gorenie i plazmokhimiya*, **18** (3), 149 (2020). (in Russian). DOI: 10.18321/cpc363
- [5] Yu. Kulagina, N. V. Latukhina, D. R. Suyundukova. *Pis'ma v ZhTF*, **49** (23), 20 (2023). (in Russian). DOI: 10.61011/PJTF.2023.23.56843.70A
- [6] O. Ziyati1, S. Abou-Obeida, Z. Walim, K.E. Boussiri. *Open Access Library J.*, **12** (4), 1–23 (2025). DOI: 10.4236/oalib.1112383
- [7] E. Fiume, G. Magnaterra, A. Rahdar, E. Verné, F. Bairo. *Ceramics*, **4** (4), 542 (2021). DOI: 10.3390/ceramics4040039

Translated by J.Savelyeva